Redox-powered autonomous unidirectional rotation about a C–C bond under enzymatic control

Jordan Berreur,[1] Olivia F. B. Watts,[†1] Theo H. N. Bulless,[†1] Nicholas T. O'Donoghue,[1] Ashley J. Winter,[1] Jonathan Clayden[*1] & Beatrice S. L. Collins[*1]

[†]These authors contributed equally.

[1]School of Chemistry, University of Bristol, Cantock's Close, Bristol, BS8 1TS, UK.

*Correspondence to: j.clayden@bristol.ac.uk; bs.lefanucollins@bristol.ac.uk.

Abstract

Living biological systems rely on the continuous operation of chemical reaction networks. These networks sustain out-of-equilibrium regimes in which chemical energy is continually converted into controlled mechanical work and motion.[1–3] Out-of-equilibrium reaction networks have also enabled the design and successful development of artificial autonomously operating molecular machines,[4,5] in which networks comprising pairs of formally—but non-microscopically—reverse reaction pathways drive controlled motion at the molecular level. In biological systems, the concurrent operation of multiple reaction pathways is enabled by the chemoselectivity of enzymes and their co-factors, and nature's dissipative reaction networks involve several classes of reactions. In contrast, the reactivity that has been harnessed to develop chemical reaction networks in pursuit of artificial molecular machines is limited to a single reaction type. Only a small number of synthetic systems exhibit chemically fuelled continuous controlled molecular-level motion,[6–8] and all exploit the same class of acylation–hydrolysis reaction. Here we show that a redox reaction network, comprising concurrent oxidation and reduction pathways, can drive chemically fuelled continuous autonomous unidirectional motion about a C–C bond in the most structurally simple synthetic molecular motor yet reported, an achiral biphenyl. The combined use of an oxidant and reductant as fuels, and the directionality of the motor, are both enabled by exploiting the enantioselectivity and functional separation of reactivity inherent to enzyme catalysis.

Continuous directional rotation about an axis is a mode of motion that underpins macroscopic machinery and will likely prove crucial for future nanoscale machines. Synthetic systems that exhibit controlled molecular-level rotary motion are dominated by the light-driven rotary molecular motors pioneered by the Feringa group over the last 25 years, in which rotatory motion occurs about a C=C double bond.[9,10] One example of autonomous chemically fuelled directional rotation about a single bond axis has been reported,[8] in which an information ratchet mechanism leads to progressive changes in angular displacement about a C–N single bond rotor. In this mechanism, non-microscopically reverse acylation and ester hydrolysis pathways generate a cyclic reaction network which is coupled to the exergonic hydrolysis of a carbodiimide fuel. Directionality is imparted to each pathway by superstoichiometric additives: a homochiral fuel (acylation) and mediator (hydrolysis). Similar acylation/hydrolysis chemical reaction networks have also been harnessed to achieve directional translational motion and to fuel out-of-equilibrium supramolecular assemblies,[5,6,11–13] but the lack of synthetic molecular motors driven by cyclic reaction networks based on alternative reactivities reflects the challenge of designing reaction networks comprising mutually compatible opposing reactions.

All life depends on redox chemistry. Concurrent oxidation and reduction reactions underpin many aspects of primary metabolism, from respiration to photosynthesis. But despite the evolution in nature of several systems that allow reduction and oxidation pathways to run concurrently, cyclic redox reaction networks have not been used to drive unidirectional motion in artificial molecular systems. In this paper we present a molecular motor in which autonomous unidirectional rotation about a C–C single bond is driven by a cyclic redox reaction network. Concurrent biocatalytic oxidation and chemical reduction reactions of a biphenyl motor create a cyclic reaction network that consumes fuel (oxygen and borane) to drive rotary motion about the biphenyl C–C bond, with directionality governed by the enantioselectivity of the oxidation biocatalyst. Isotopically labelled fuels and interrupted fuelling studies confirm the continuous operation of the rotary motor, and novel isotopomer methods confirm the directionality of rotation.

Our design builds upon an archetypal cyclic reaction network in synthetic chemistry: cyclic deracemization.[14] Cyclic deracemizations enable the contra-thermodynamic enrichment of one enantiomer from a racemic mixture through the operation of a dissipative cyclic reaction network.[15–28] For example, in the seminal redox-driven cyclic deracemization from Turner and

coworkers shown in Figure 1a,[29] enantioselective oxidation of a racemic pair of amines is coupled with non-stereoselective reduction, leading to enrichment in the less reactive of the two amine enantiomers. Concurrent oxidation and reduction is achieved by recourse to an oxidation biocatalyst (monoamine oxidase) that can function in the presence of a reducing agent, in this case ammonia borane ($H_3N{\cdot}BH_3$).

A related, but as yet unexplored, model for cyclic deracemization passes not through a transient achiral intermediate (the imine in Figure 1a) but instead through a transient state that consists of a pair of rapidly interconverting enantiomers. A model for such a deracemization is shown in Figure 1b. Oxidation of the chiral atropisomeric diol **1** would give hydroxyaldehyde **2**, which is expected to racemise rapidly at room temperature owing to a bonding interaction between the phenolic hydroxyl group and the aldehyde carbonyl (shown in square brackets). Covalent bonding interactions that lower energy barriers to bond rotation provide the basis for Bringmann's 'lactone' method and other more recent strategies for the enantioselective synthesis of atropisomers,[30,31] and related covalent bonding interactions are exploited in the rotary motor of Leigh and co-workers and other stepwise rotary molecular motors.[8,32–35] Transient non-covalent bonding interactions,[36] as proposed for hydroxyaldehyde **2**, have been used extensively in the asymmetric synthesis of atropisomers through dynamic kinetic resolution methods using organo-, transition metal and enzymatic catalysis.[31,37,38]

In analogy to Turner's cyclic deracemization of a point chiral centre (Figure 1a),[29] deracemization of atropisomeric **1** occurs if the oxidation to hydroxyaldehyde **2** proceeds enantioselectively and is coupled to a non-selective reduction back to the diol **1**. Such an atropisomeric deracemization is also accompanied by net directional motion: if the oxidation of **1** to **2** is enantioselective, the rapidly interconverting mixture of enantiomeric conformers of **2** is approached selectively from one direction, and every transformation of (S_a)-**1** to (R_a)-**1** results from a 180° anticlockwise rotation of the upper ring, as viewed from above, indicated by the curved arrow.

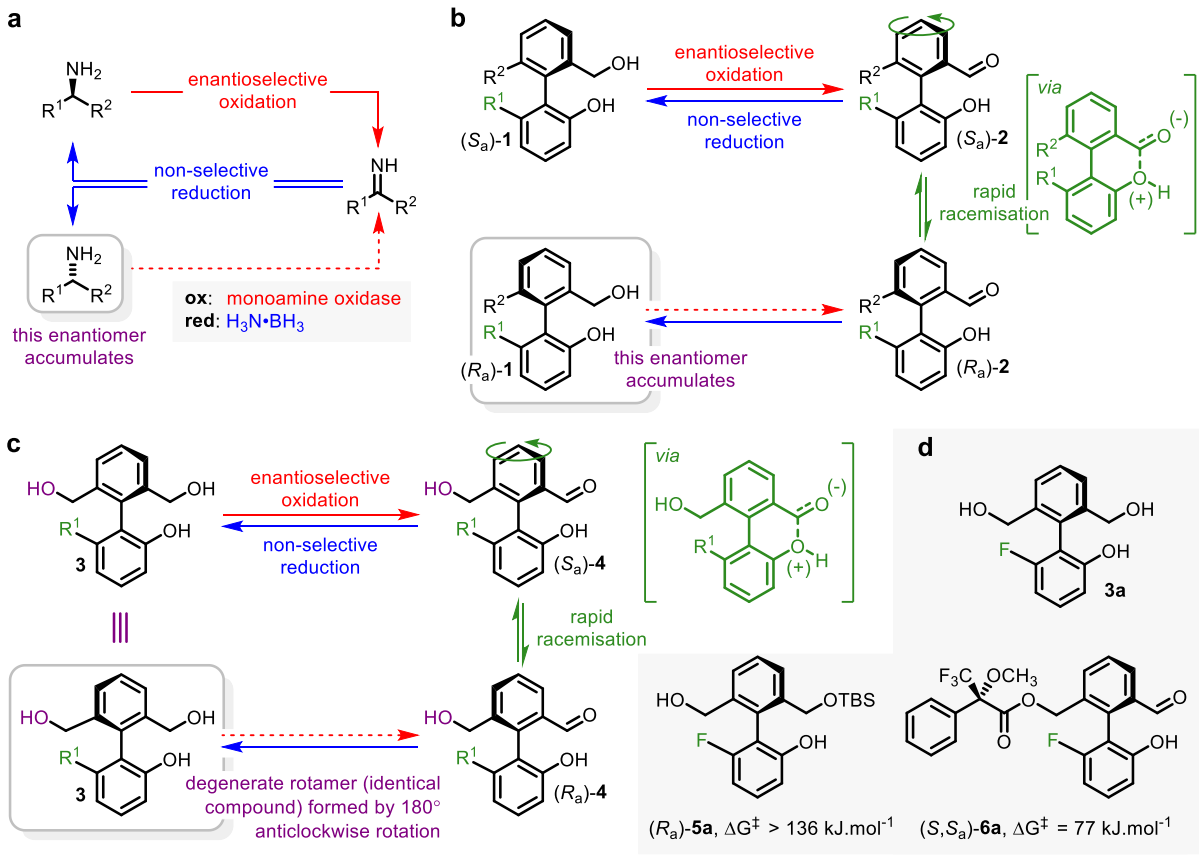

Fig. 1 | Cyclic deracemization as a model for unidirectional rotation. a Cyclic deracemization of point-chiral amines by way of an achiral imine, coupling enantioselective biocatalytic oxidation with non-selective reduction using ammonia borane.[29] **b** Cyclic deracemization of an atropisomeric biphenyl by way of a pair of rapidly interconverting enantiomeric conformers. **c** Design for a unidirectional rotary molecular motor. **d** Motor **3a** and desymmetrized derivatives (R_a)-**5a** and (S,S_a)-**6a**. Stereochemical assignment assumes that R^1 has higher priority than OH and R^2 has lower priority than CH_2OH.

In Figure 1c, we outline how one small change to the biphenyl deracemization substrate **1** reveals a simple design for a unidirectional rotary molecular motor. The same cyclic reaction network is applied to closely analogous molecule **3**, which has two hydroxymethyl substituents in the *ortho* positions of the upper ring (Figure 1c). Triol **3** is now achiral by virtue of the plane of symmetry that bisects the upper ring. Enantioselective oxidation desymmetrizes triol **3** to give an enantioenriched sample of chiral monoaldehyde (S_a)-**4** that itself undergoes rapid racemisation due to the bonding interaction between the phenolic hydroxyl group and the aldehyde carbonyl (shown in square brackets). From monoaldehyde **4**, the concurrent non-selective reduction does not return the enantiomer of the starting triol, because this achiral triol is, by definition, superimposable upon its mirror image. Instead, it simply returns the starting material **3**, ready to undergo another redox cycle. Crucially, however, a proportion of those triol molecules **3** that return from the oxidation-reduction cycle have undergone net 180°

anticlockwise rotation of the upper ring during the racemisation of the transient monoaldehyde intermediate **4** (with the remainder having undergone no net rotation). Thus, after one oxidation-reduction cycle, a proportion of triol **3** is returned in the form of a chemically indistinguishable (degenerate) rotamer in which the hydroxymethyl groups have exchanged positions via 180° anticlockwise rotation. Oxidation of the second hydroxymethyl group (shown in purple) of **3** allows this rotated fraction of the starting material to enter the redox cycle a second time, and again a fraction will undergo 180° anticlockwise rotation. The dissipative cyclic redox reaction network thus no longer supports a deracemization; instead, it drives continuous autonomous net directional motion. We shall now describe how this design for a redox-driven molecular motor was reduced to practice.

The biphenyl rotary motor requires a symmetrically substituted phenyl 'rotor' ring with hydroxymethyl groups in each *ortho* position, and a phenolic 'stator' ring substituted by R^1 in the final *ortho* position. The nature of substituent R^1 allows the rotational barriers of the reduced and oxidised states of the motor (triol **3** and monoaldehyde **4**) to be adjusted for optimal function. We identified *ortho*-fluoro triol **3a** (R^1 = F), readily prepared through a five-step synthetic sequence, as a promising motor candidate with a configurationally stable reduced state **3a** and a configurationally labile oxidised state **4a** (Figure 1d). Rotational barriers of **3a** and **4a** were estimated using desymmetrized derivatives.[39] Silylation of **3a** with a $SiMe_2t$-Bu (TBS) group and chromatographic resolution gave an enantioenriched sample of desymmetrized triol **5a** that showed no detectable racemisation after two days at 100 °C in toluene ($\Delta G^{\ddagger}_{rot}$ > 136 kJ mol^{-1}; Supplementary Information Section 7.3). Acylation of **4a** with Mosher's acyl chloride **7** gave ester **6a**,[40] whose axial diastereoisomers show resolved signals by ^{1}H and ^{19}F NMR spectroscopy. ^{19}F NMR EXSY analysis of the mixture of diastereoisomers of **6a** indicates that the resolved signals undergo chemical exchange and reveals a barrier to rotation $\Delta G^{\ddagger}_{rot}$ ~ 77 kJ mol^{-1} in 2:1 DMSO:D_2O (Supplementary Information Section 7.3).

A cyclic reaction network that would allow concurrent enantioselective oxidation of achiral **3a** and non-selective reduction of **4a** was developed by using the cyclic deracemization of chiral analogue **1a** as a model. Alcohol dehydrogenases (ADHs)[41] have been used by Kroutil and coworkers in cyclic reaction networks leading to the deracemization of point-chiral alcohols,[42,43] and have also been used in the enantioselective synthesis of chiral biaryls through both desymmetrization and dynamic kinetic resolution processes.[44–47] Inspired by these studies,

as well as Turner's seminal report of concurrent biocatalytic oxidation and chemical reduction pathways in the deracemization of benzylic amines,[29] we screened a library of ADHs in conjunction with excess ammonia borane for the deracemization of **1a** (Figure 2). The ADH-catalysed oxidation of the benzylic alcohol moiety was realised using NADP as co-factor, an NADPH oxidase (PRO-NOX(001) or YcnD) as the co-factor recycling enzyme,[48,49] and molecular oxygen as the terminal oxidant. We quickly identified ADH 159 as an effective catalyst for deracemization: addition of ten equivalents of ammonia borane at the outset of the ADH-catalysed oxidation led to a reaction profile consisting of almost exclusively **1a** with an ee of 38% after 54 hours (Figure 2a, Entry 4; the sense of enantioselectivity of the ADH was established from its action on a known substrate, see Supplementary Information Section 4 for details). Further optimisation of the recycling system, pH, and temperature provided (R_a)-**1a** in 95% ee after 24 hours (Figure 2a, Entry 9; see Supplementary Information Section 5 for full optimisation details). Monitoring the reaction over time (Figure 2b) established that the ee increased over ~24 h as **1a** underwent repetitive cycles of oxidation and reduction.

a

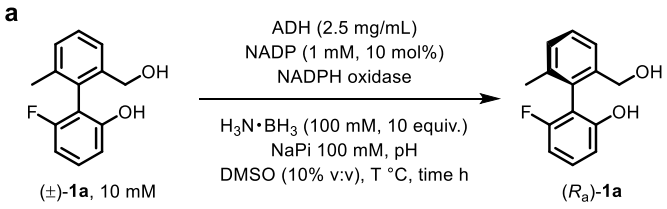

(±)-**1a**, 10 mM (R_a)-**1a**

Entry	ADH	NADPH oxidase	T / °C	pH	ee of **1a**
1	19	PRO-NOX(001)	30	7	14
2	20	PRO-NOX(001)	30	7	16
3	27	PRO-NOX(001)	30	7	0
4	159	PRO-NOX(001)	30	7	38
5	159	PRO-NOX(001)	30	8	65
6	159	PRO-NOX(001)	40	8	36
7	159	YcnD	30	8	96
8	159	YcnD	25	8	96
9	159[a]	YcnD	25	8	95[b]

b

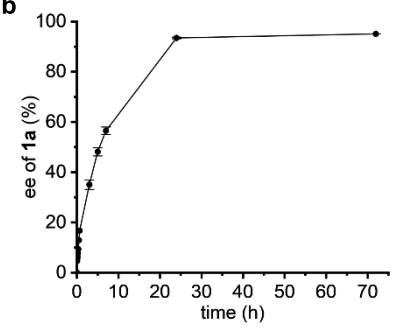

Fig. 2 | Deracemization of biaryl 1a. **a** Optimization of deracemization of **1a**: (±)-**1a** (10 mM), ADH (2.5 mg/mL), NADP (1 mM, 10 mol%), NADPH oxidase (either PRO-NOX(001) (1 mg/mL) or YcnD (12 μM)), NaPi (100 mM), DMSO (10% v:v), $H_3N{\cdot}BH_3$ (100 mM, 10 equiv.), ee analysis performed by HPLC at 40–55 h; [a] ADH 159 (5.0 mg/mL); [b] analysis performed at 24 h. **b** ee of **1a** over time for conditions in Entry 9.

Critically, the deracemization of **1a** confirms the operation of the proposed redox cyclic chemical reaction network: enantiomeric enrichment can arise only through the continuous concurrent operation of non-microscopically reverse pathways between **1a** and **2a**, the

oxidation and reduction pathways. In addition, this highly effective deracemization of **1a** provides insight into the hierarchy of rates that characterises the cyclic reaction network: in order for deracemization to occur, it is necessary that the interconversion of the enantiomeric conformers of **2a** (i.e., the enantiomerization of **2a**) occurs faster than the reduction of **2a** back to **1a**. Both the reduction and enantiomerization of **2a** must also occur faster than the oxidation of **1a**. These kinetic constraints can be expressed as a hierarchy of rates, $r_{enant} > r_{red} > r_{ox(Ra,Sa)}$. Finally, the deracemization of **1a** also confirms that the oxidation is stereoselective, i.e., $r_{ox(Sa)}/r_{ox(Ra)} \neq 1$.

Having established an effective deracemization of **1a**, we set about constructing an analogous cyclic redox reaction network under which motor candidate **3a** would undergo rotary motion. We again screened a small library of ADHs and identified ADH 19 as an effective catalyst for the oxidation of triol **3a** to monoaldehyde **4a**. **3a** was then treated with ADH 19 under the conditions of the cyclic reaction network: addition of 10 equivalents of ammonia borane at the outset of the reaction resulted in a reaction mixture comprising almost exclusively **3a** after 48 hours (Figure 3a). When ammonia trideuteroborane ($H_3N{\cdot}BD_3$) was used in place of ammonia borane, deuterium was gradually incorporated at the benzylic positions of **3a** (Figure 3b), confirming that, under these conditions, chemically unchanged motor **3a** is undergoing multiple cycles of oxidation and reduction.

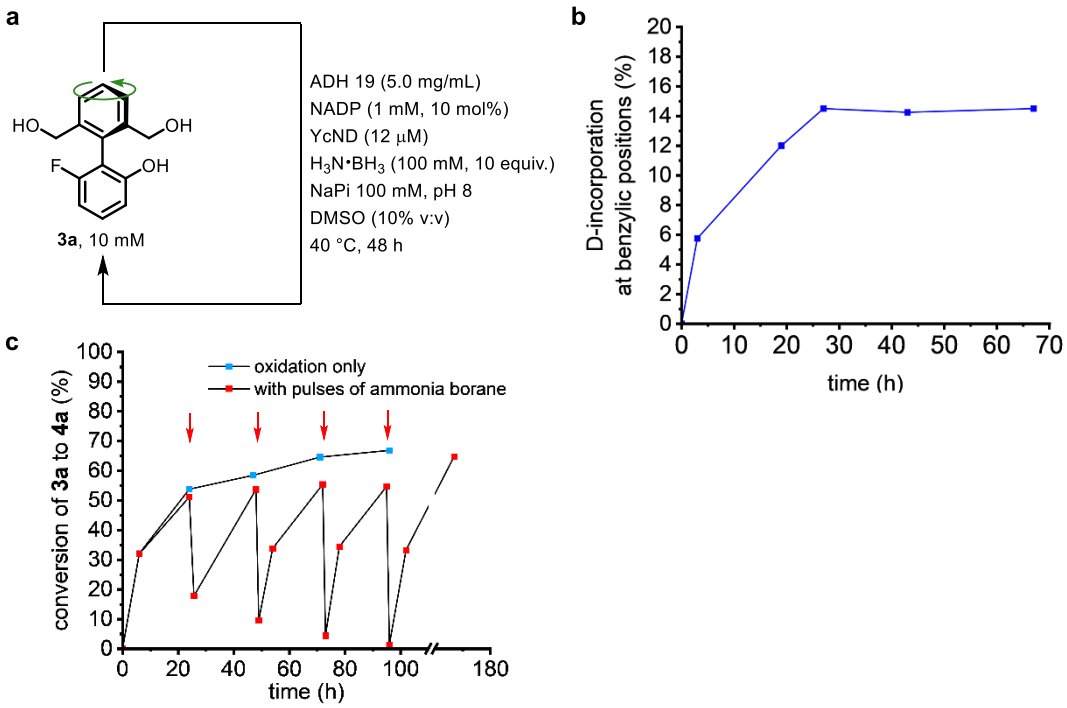

Fig. 3 | Operation of motor 3a under the cyclic redox reaction network. a Motor **3a** under the conditions of the cyclic redox reaction network: **3a** (10 mM), ADH 19 (25 mg/mL), NADP (5 mM, 50 mol%), YcnD (60 μM), $H_3N{\cdot}BH_3$ (100 mM, 10 equiv.), NaPi (100 mM, pH 7.0), DMSO (10% v:v), 40 °C, 48 h. **b** Ammonia trideuteroborane ($H_3N{\cdot}BD_3$) in place of ammonia borane ($H_3N{\cdot}BH_3$) in the cyclic redox reaction network leads to deuterium incorporation at the benzylic positions of **3a**. **c** Blue squares: oxidation of motor **3a** to monoaldehyde **4a** under standard conditions: **3a** (10 mM), ADH 19 (25 mg/mL), NADP (5 mM, 50 mol%), YcnD (60 μM), NaPi (100 mM, pH 7.0), DMSO (10% v:v), 40 °C; red squares: pulses of $H_3N{\cdot}BH_3$ (2 mM, 0.2 equiv.) added at 24, 48, 72 and 96 h (addition timepoints depicted with red arrows).

The continued viability of the cyclic redox reaction network over extended periods of time was confirmed by subjecting **3a** to sub-stoichiometric pulses of ammonia borane at regular intervals, rather than a large excess at the outset of the reaction (Figure 3c). At the outset of the reaction, **3a** was subjected to the standard oxidation conditions and after 24 hours, 51% conversion to monoaldehyde **4a** was observed. A pulse of ammonia borane (approx. 0.2 equivalents) was added at 24 hours, followed by analysis at 1 hour (18% conversion to monoaldehyde **4a**) and 24 hours (54% conversion to **4a**), confirming that the oxidation system (ADH 19, NADP, and YcnD) was viable for at least 24 hours. A further 3 pulses of ammonia borane (3 x approx. 0.2 equivalents) were applied at 24 hour intervals. After each pulse, monoaldehyde **4a** was regenerated in similar conversions (approx. 50%), confirming the viability of the oxidation system over at least 96 hours. By monitoring the background conversion of ammonia borane to boric acid ($B(OH)_3$), we also confirm that **3a** accelerates the fuel-to-waste conversion (see Supplementary Information Section 8 for details).

The experiments detailed in Figure 3 confirm that **3a** is a substrate for the cyclic redox reaction network, that **3a** undergoes multiple sequential cycles of oxidation and reduction under the standard operating conditions (i.e., $[H_3N{\cdot}BD_3]_0$ = 100 mM), and that the oxidation system remains viable over at least 96 hours. Directional rotation of the motor requires, in addition, the rate of enantiomerization of **4a** to be greater than the rate of its reduction (i.e., $r_{enant} > r_{red}$); if this condition is not met, the motor oscillates between the two redox states **3a** and **4a** but without accompanying rotation about the biaryl axis. Furthermore, effective motor operation requires that the rate of oxidation of **3a** is the slowest of the three constituent steps ($r_{enant} > r_{red} > r_{ox(Ra,Sa)}$) and that the oxidation of **3a** proceeds stereoselectively, i.e., $r_{ox(Sa)}/r_{ox(Ra)} \neq 1$. For the deracemization of **1a**, the emergence of enantiomeric enrichment proved that these kinetic constraints were met. But directional rotation of **3a** has no equivalent stereochemical consequence, so in order to confirm that the motor is operating, we evaluated these rates independently.

To confirm the hierarchy of rates, $r_{enant} > r_{red} > r_{ox(Ra,Sa)}$, we determined each rate separately under conditions matching as closely as possible the operating conditions of the motor. The rate of enantiomerization, r_{enant}, (i.e., the rate of interconversion of (R_a)-**4a** and (S_a)-**4a**) was estimated from the barrier to rotation about the equivalent biaryl axis of the Mosher's ester derivative (*S*)-**6a** in a mixture of D_2O and DMSO: r_{enant}((*S*)-**6a**) = 9.4 x 10^{-1} · [**4a**] mM.s^{-1} (Figure 1d). The rate of the reduction of **4a**, r_{red}, was determined by monitoring the reduction of **4a** to **3a** in a NaPi (100 mM, pH 7.0) / DMSO (10% v:v) mixture at 313 K using UV/vis spectroscopy (see Supplementary Information Section 7.2 for full details) to give r_{red} = 2.4 x 10^{-3} · $[H_3N{\cdot}BH_3]$ · [**4a**] mM.s^{-1}. The undetectably low concentration of **4a** at the steady state of the cyclic redox reaction network ($r_{red} >> r_{ox(Ra,Sa)}$: see below) precludes the determination of absolute values of r_{enant} and r_{red}. However, rotary motor operation is contingent only on the *relative* rates of r_{enant} and r_{red}, and under the standard operating conditions (i.e., $[H_3N{\cdot}BH_3]_0$ = 100 mM), r_{red}/r_{enant} = 0.26 (< 1, as required; see Supplementary Information Section 7 for details). The rate of oxidation of **3a** ($r_{ox(Ra,Sa)}$) was determined by monitoring the oxidation of **3a** to **4a** under the operating conditions of the motor using HPLC. In the initial stages of the oxidation reaction, [**3a**] >> [ADH], and the enzyme can be considered to be operating at V_{max} according to Michaelis-Menten kinetics. The resulting pseudo-zero order plot gives $r_{ox(Ra,Sa)}$ = 7.63 x 10^{-4} mM.s^{-1}. Without absolute values for r_{enant} or r_{red} we cannot compare them with this value numerically, but we make the assumption that $r_{red} >> r_{ox(Ra,Sa)}$, since **3a** is the resting of

the cyclic redox reaction network. The pseudo-zero order reaction kinetics noted in the determination of $r_{ox(Ra,Sa)}$ remain valid during the operation of the cyclic redox reaction network because the concentration of **3a** remains constant, being rapidly replenished by the excess of ammonia borane. Under the standard operating conditions of the motor, the rates of the three constituent processes that underpin rotary motor operation do thus indeed conform to the required hierarchy of rates, $r_{enant} > r_{red} > r_{ox(Ra,Sa)}$.

The final proof that **3a** undergoes continuous directional rotation under the conditions of the cyclic redox reaction network requires evidence that the oxidation of **3a** proceeds stereoselectively, i.e., that $r_{ox(Sa)}/r_{ox(Ra)} \neq 1$. This information cannot be provided by direct observation of enantiomeric enrichment in either starting material or product, because **3a** is achiral, and (R_a)-**4a** and (S_a)-**4a** racemise too fast for analysis of the enantiomeric ratio. Enantioselectivity can nonetheless be deduced from oxidations of enantiopure isotopomers (S_a)-D_2-**3a** and (R_a)-D_2-**3a**, which were made with 95% deuterium incorporation by methods described in the Supplementary Information and whose absolute configuration was determined as described in the SI. As depicted in Figure 4a, oxidation of (S_a)-D_2-**3a** generates monoaldehyde **4a** in which the deuterium label (CD_2 or CD) is distributed between the aldehydic CDO and benzyl alcoholic CD_2OH positions in a ratio of 93:7 (^{1}H NMR spectroscopy). Conducting the experiment with the isotopomer, (R_a)-D_2-**3a**, gives a ratio of deuterium incorporation at the aldehydic and benzylic positions of 5:95. The enantioselectivity of the oxidation, $r_{ox(Sa)}/r_{ox(Ra)}$, determines the ratio of deuterium incorporation (e.g., for (S_a)-D_2-**3a**, $r_{ox(Sa)}/r_{ox(Ra)}$ = aldehydic signals labelled with D / benzylic signals labelled with D_2), where the difference between the ratios and the conversions observed for the two isotopomers arises from the kinetic isotope effect (KIE) of the oxidation. Together, these experiments indicate that oxidation of unlabelled motor **3a** to monoaldehyde **4a** proceeds with an ee that falls in the range 85.7 ± 6.1% ee to 89.5 ± 2.7% ee, confirming that $r_{ox(Sa)}/r_{ox(Ra)} \neq 1$. This experiment provides the first direct evidence of directional motion in an operational single bond rotary motor.

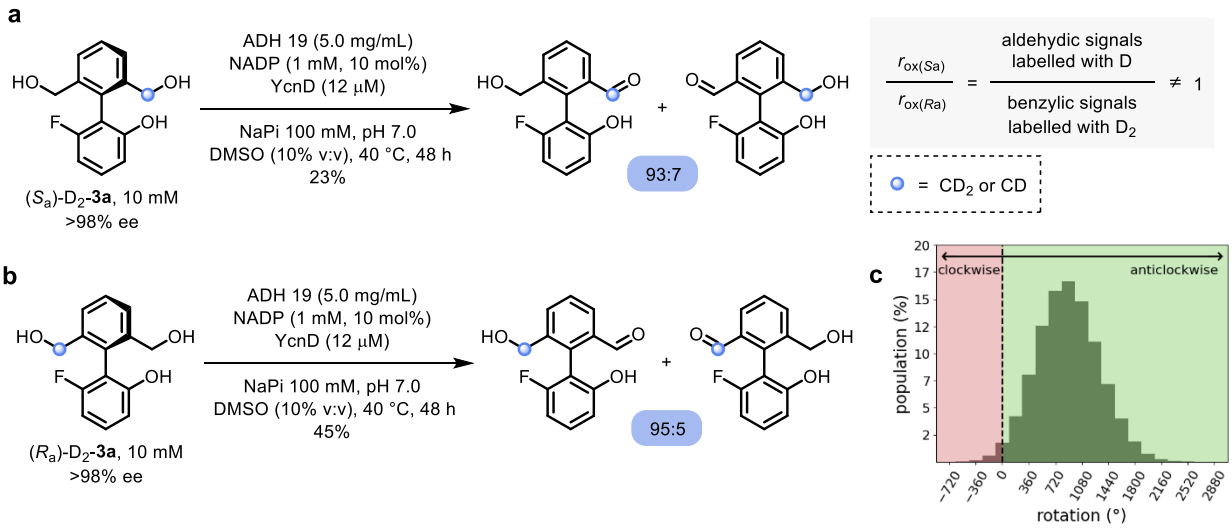

Fig. 4 | Proof of directional rotation for motor 3a. a Oxidation of (S_a)-D$_2$-**3a** ((S_a)-D$_2$-**3a** (10 mM, >98% ee), ADH 19 (5.0 mg/mL), NADP (1 mM, 10 mol%), YcnD (12 μM), NaPi (100 mM, pH 7.0), DMSO (10% v:v), 40 °C, 48 h), analysis of deuterium distribution at aldehydic CDO and benzylic CD$_2$OH positions, and example determination of $r_{ox(Sa)}/r_{ox(Ra)}$. **b** Oxidation of (R_a)-D$_2$-**3a** ((R_a)-D$_2$-**3a** (10 mM, >98% ee), ADH 19 (5.0 mg/mL), NADP (1 mM, 10 mol%), YcnD (12 μM), NaPi (100 mM), pH 7.0, DMSO (10% v:v), 40 °C, 48 h) and analysis of deuterium distribution at benzylic CD$_2$OH and aldehydic CDO positions. **c** Histogram illustrating the distribution of the net angles of rotation of 10^6 simulated molecules of **3a** after 48 h of operation (see Supplementary Information Section 10 for details).

The experiments detailed in Figure 3, the confirmation of a hierarchy of rates, and this direct observation of enantioselectivity in one of the constituent steps of the cyclic redox reaction network, confirm that under the standard reaction conditions, biphenyl **3a** undergoes continuous net directional rotation about the C–C single bond. With the oxidation of **3a** to **4a** proceeding at a rate of $r_{ox(Ra,Sa)} = 7.63 \times 10^{-4}$ mM.s^{-1} and assuming an average enantioselectivity of 87.6% ee, we determine that for a statistically relevant population of motor **3a**, the mean number of 360° rotations after 48 h of operation will be 2.48 (Figure 4c). The rotational frequency of biphenyl motor **3a** could be increased by optimising the rate and/or enantioselectivity of the oxidation, and by developing a cyclic redox reaction network comprising stereoselective oxidation *and* reduction pathways. Cyclic reaction networks comprising enantioselective biocatalytic reactions for both oxidation and reduction have been reported for the deracemization of point chiral alcohols by Kroutil and co-workers.[42,50]

In summary, rotary motor **3a** undergoes autonomous directional rotary motion about a C–C single bond, powered by a biocatalytic cyclic redox reaction network. Our studies confirm **3a**

as a substrate for the cyclic redox reaction network; a kinetic analysis establishes that the system conforms to a hierarchy of rates required for rotary rather than oscillatory motion; deuterium isotopomer studies confirm the stereoselectivity of the biocatalytic oxidation of **3a** and allow, for the first time, the directionality of rotary motion of a functioning single bond molecular motor to be confirmed. Through this report of the first redox driven single bond rotary motor, biocatalysis emerges as a powerful tool for the design and development of autonomously operating chemically fuelled molecular motors.

Data availability The data that support the findings of this study are available within the paper and its Supplementary Information.

Acknowledgements We thank the Leverhulme Trust (Research Project Grant RPG-2020-031), the Royal Society (RS; University Research Fellowship to B.S.L.C.; URF/R1/180592), the European Research Council (ERC; Advanced Grant 883786 to J.C.), the Engineering and Physical Sciences Research Council (EPSRC; studentships to O.F.B.W. and N.T.O.D. through the Bristol Centre for Doctoral Training in Technology-Enhanced Chemical Synthesis; EP/S024107/1), the Biotechnology and Biological Sciences Research Council (BBSRC; advanced NMR techniques through awards BB/V019163/1 and BB/W008823/1), for funding, Johnson Matthey for the generous gift of alcohol dehydrogenases (ADHs) and cofactors, Paul Lawrence, Chris Williams and Jean-Paul Heeb for support with NMR experiments, and Samantha Staniland of AstraZeneca for valuable discussions.

Author contributions B.S.L.C and J.C. conceived the project. J.B, O.F.B.W., T.H.N.B. and N.T.O.D. designed and carried out the experiments. A.J.W. carried out the expression and purification of the NADPH oxidase YcnD. B.S.L.C and J.C. directed the research. All authors contributed to the analysis of the results and the writing of the manuscript.

Competing interests The authors declare no competing interests.

Additional information

Supplementary information The online version contains supplementary material available at xxx.

Correspondence and requests for materials should be addressed to B.S.L.C and J.C.

References

[1] Schliwa, M., Woehlke, G. Molecular motors. *Nature* **422**, 759–765 (2003).

[2] Boyer, P. D. Energy, Life, and ATP (Nobel Lecture 1997). *Angew. Chem. Int. Ed.* **37**, 2296–2307 (1998).

[3] Fletcher, D. A., Mullins, R. D. Cell mechanics and the cytoskeleton. *Nature* **463**, 485–492 (2010).

[4] Kassem, S. *et al.* Artificial Molecular Motors. *Chem. Soc. Rev.* **46**, 2592–2621 (2017).

[5] Borsley, S., Leigh, D. A., Roberts, B. M. W. Chemical fuels for molecular machinery. *Nat. Chem.* **14**, 728–738 (2022).

[6] Wilson, M. R. *et al.* An autonomous chemically fuelled small-molecule motor. *Nature* **534**, 235–240 (2016).

[7] Borsley, S., Leigh, D. A., Roberts, B. M. W. A Doubly Kinetically-Gated Information Ratchet Autonomously Driven by Carbodiimide Hydration. *J. Am. Chem. Soc.* **143**, 4414–4420 (2021).

[8] Borsley, S., Kreidt, E., Leigh, D. A., Roberts, B. M. W. Autonomous fuelled directional rotation about a covalent single bond. *Nature* **604**, 80–85 (2022).

[9] Koumura, N, Zijlstra, R. W. J., van Delden, R. A., Harada, N., Feringa, B. L. Light-driven monodirectional molecular rotor. *Nature* **401**, 152–155 (1999).

[10] Roke, D., Wezenberg, S. J., Feringa, B. L. Molecular rotary motors: Unidirectional motion around double bonds. *Proc. Natal. Acad. Sci.* **115**, 9423–9431 (2018).

[11] Kariyawasam, L. S., Hartley, C. S. Dissipative Assembly of Aqueous Carboxylic Acid Anhydrides Fueled by Carbodiimides. *J. Am. Chem. Soc.* **139**, 11949–11955 (2017).

[12] Rieβ, B., Grötsch, R. K., Boekhoven, J. The Design of Dissipative Molecular Assemblies Driven by Chemical Reaction Cycles. *Chem* **6**, 552–578 (2020).

[13] Kariyawasam, L. S., Hossain, M., M., Hartley, C. S. The Transient Covalent Bond in Abiotic Nonequilibrium Systems. *Angew. Chem. Int. Ed.* **60**, 12648–12658 (2021).

[14] Huang, M., Pan, T., Jiang, X., Luo, S. Catalytic Deracemization Reactions. *J. Am. Chem. Soc.* **145**, 10917–10929 (2023).

[15] Lackner, A. D., Samant, A. V., Toste, F. D. Single-Operation Deracemization of 3H-Indolines and Tetrahydroquinolines Enabled by Phase Separation. *J. Am. Chem. Soc.* **135**, 14090–14093 (2013).

[16] Ji, Y., Shi, L., Chen, M.-W., Feng, G.-S., Zhou, Y.-G. Concise Redox Deracemization of Secondary and Tertiary Amines with a Tetrahydroquinoline Core via a Nonenzymatic Process. *J. Am. Chem. Soc.* **137**, 10496–10499 (2015).

[17] Wan, M., Sun, S., Li, Y., Liu, L. Organocatalytic Redox Deracemization of Cyclic Benzylic Ethers Enabled by An Acetal Pool Strategy. *Angew. Chem. Int. Ed.* **56**, 5116–5120 (2017).

[18] Hölzl-Hobmeier, A. *et al*. Catalytic deracemization of chiral allenes by sensitized excited with visible light. *Nature* **564**, 240–243 (2018).

[19] Plaza, M., Groβkopf, J., Breitenlechner, S., Bannwarth, C., Bach, T. Photochemical Deracemization of Primary Allene Amides by Triplet Energy Transfer: A Combined Synthetic and Theoretical Study. *J. Am. Chem. Soc.* **143**, 11209–11217 (2021).

[20] Kratz, T. *et al*. Photochemical Deracemization of Chiral Alkenes via Triplet Energy Transfer. *J. Am. Chem. Soc.* **144**, 10133–10138 (2022).

[21] Groβkopf, J. *et al*. Photochemical Deracemization at sp^3-Hybridized Carbon Centres via a Reversible Hydrogen Atom Transfer. *J. Am. Chem. Soc.* **143**, 21241–21245 (2021).

[22] Zhang, C. *et al*. Catalytic α-Deracemization of Ketones Enabled by Photoredox Deprotonation and Enantioselective Protonation. *J. Am. Chem. Soc.* **143**, 13393–13400 (2021).

[23] Shin, N. Y., Ryss, J. M., Zhang, X., Miller, S. J., Knowles, R. R. Light-driven deracemization enabled by excited-state electron transfer. *Science* **366**, 364–369 (2019).

[24] Huang, M., Zhang, L., Pan, T., Luo, S. Deracemization through photochemical *E*/*Z* isomerization of enamines. *Science* **375**, 869–874 (2022).

[25] Gu, Z. *et al*. Deracemization through Sequential Photoredox-Neutral and Chiral Brønsted Acid Catalysis. *Angew. Chem. Int. Ed.* **61**, e202211241 (2022).

[26] Chen, Q. *et al.* Light-driven redox deracemization of indolines and tetrahydroquinolines using a photocatalyst coupled with chiral phosphoric acid. *Chem. Sci.* **14**, 1715–1723 (2023).

[27] Zhang, Z., Hu, X. Visible-Light-Driven Catalytic Deracemization of Secondary Alcohols. *Angew. Chem. Int. Ed.* **60**, 22833–22838 (2021).

[28] Wen, L. *et al*. Multiplicative enhancement of stereoenrichment by a single catalyst for deracemization of alcohols. *Science* **382**, 458–464 (2023).

[29] Alexeeva, M., Enright, A., Dawson, M. J., Mahmoudian, M., Turner, N. J. Deracemization of α-Methylbenzylamine Using an Enzyme Obtained by In Vitro Evolution. *Angew. Chem. Int. Ed.* **41**, 3177–3180 (2002).

[30] Bringmann, G. *et al*. Atroposelective Synthesis of Axially Chiral Biaryl Compounds. *Angew. Chem. Int. Ed.* **44**, 5384–5427 (2005).

[31] Cheng, J. K., Xiang, S.-H., Li, S., Ye, L., Tan, B. Recent Advances in Catalytic Asymmetric Construction of Atropisomers. *Chem. Rev.* **121**, 4805–4902 (2021).

[32] Fletcher, S. P., Dumur, F., Pollard, M. M., Feringa, B. L. A Reversible, Unidirectional Molecular Rotary Motor Driven by Chemical Energy. *Science* **310**, 80–82 (2005).

[33] Collins, B. S. L., Kistemaker, J. C. M., Otten, E. Feringa, B. L. A chemically powered unidirectional rotary molecular motor based on a palladium redox cycle. *Nat. Chem.* **8**, 860–866 (2016).

[34] Zhang, Y. *et al*. A Chemically Driven Rotary Molecular Motor Based on Reversible Lactone Formation with Perfect Unidirectionality. *Chem* **6**, 2420–2429 (2020).

[35] Zwick, P., Troncossi, A., Borsley, S., Vitorica-Yrezabel, I. J., Leigh, D. A. Stepwise Operation of a Molecular Rotary Motor Driven by an Appel Reaction. *J. Am. Chem. Soc.* doi.org/10.1021/jacs.3c10266 (2024).

[36] Chen, H. *et al*. Effects of n→π* Orbital Interactions on Molecular Rotors: The Control and Switching of Rotational Pathway and Speed. *Org. Lett.* **23**, 231–235 (2021).

[37] Chan, V., Kim, J. G., Jimeno, C., Carroll, P. J., Walsh, P. J. Dynamic Kinetic Resolution of Atropisomeric Amides. *Org. Lett.* **6**, 2051–2053 (2004).

[38] Roos, C. B. *et al*. Stereodynamic Strategies to Induce and Enrich Chirality of Atropisomers at a Late Stage. *Chem. Rev.* **123**, 10641–10727 (2023).

[39] Heeb, J.-P., Clayden, J., Smith, M. D., Armstrong, R. J. Interrogating the configurational stability of atropisomers. *Nat. Protoc.* **18**, 2745–2771 (2023).

[40] Dale, J. A., Mosher, H. S. Nuclear Magnetic Resonance Enantiomer Reagents. Configurational Correlations via Nuclear Magnetic Resonance Chemical Shifts of Diastereomeric Mandelate, *O*-Methylmandelate, and α-Methoxy-α-trifluoromethylphenylacetate (MTPA) Esters. *J. Am. Chem. Soc.* **95**, 512–519 (1973).

[41] Dong, J. *et al*. Biocatalytic Oxidation Reactions: A Chemist's Perspective. *Angew. Chem. Int. Ed.* **57**, 9238–9261 (2018).

[42] Voss, C. V. *et al*. Orchestration of Concurrent Oxidation and Reduction Cycles for Stereoinversion and Deracemisation of *sec*-Alcohols. *J. Am. Chem. Soc.* **130**, 13969–13972 (2008).

[43] Voss, C. V., Gruber, C. C., Kroutil, W. Deracemisation of Secondary Alcohols via Biocatalytic Stereoinversion. *Synlett* **7**, 991–998 (2010).

[44] Staniland, S. *et al*. Enzymatic Desymmetrising Redox Reactions for the Asymmetric Synthesis of Biaryl Atropisomers. *Chem. Eur. J.* **20**, 13084–13088 (2014).

[45] Staniland, S. *et al*. Biocatalytic Dynamic Kinetic Resolution for the Synthesis of Atropisomeric Biaryl N-Oxide Lewis Base Catalysts. *Angew. Chem. Int. Ed.* **55**, 10755–10759 (2016).

[46] Rodríguez-Salamanca, P. *et al*. Biocatalytic Atroposelective Synthesis of Axially Chiral N-Arylindoles via Dynamic Kinetic Resolution. *ACS Catal.* **13**, 659–664 (2023).

[47] Coto-Cid, J. M. *et al*. Atroposelective Synthesis of 2-(Quinolin-8-yl)benzyl Alcohols by Biocatalytic Dynamic Kinetic Resolutions. *Adv. Synth. Catal.* doi.org/10.1002/adsc.202301310 (2024).

[48] Rehn, G., Pedersen, A. T., Woodley, J. M. Application of NAD(P)H oxidase for cofactor regeneration in dehydrogenase catalyzed oxidations. *J. Mol. Catal. B: Enzymatic* **134**, 331–339 (2016).

[49] Morokutti, A. *et al*. Structure and Function of YcnD from Bacillus subtilis, a Flavin-Containing Oxidoreductase. *Biochemistry* **44**, 13724–13733 (2005).

[50] Holmann, F., Opperman, D. J., Paul, C. E. Biocatalytic Reduction Reactions for a Chemist's Perspective. *Angew. Chem. Int. Ed.* **60**, 5644–5665 (2021).